MOX-Report No. 05/2020

An adaptive curved virtual element method for the statistical homogenization of random fibre-reinforced composites

Artioli, E.; Beiraoda Veiga, L.; Verani, M.

MOX, Dipartimento di Matematica
Politecnico di Milano, Via Bonardi 9 - 20133 Milano (Italy)

mox-dmat@polimi.it http://mox.polimi.it

An adaptive curved virtual element method for the statistical homogenization of random fibre-reinforced composites

E. Artioli[a,*], L. Beirão da Veiga[b], M. Verani[c]

[a] *Department of Civil Engineering and Computer Science, University of Rome Tor Vergata, via del Politecnico 1, Rome*
[b] *Department of Mathematics and Applications, University of Milano Bicocca, Milan*
[c] *MOX-Department of Mathematics, Politecnico di Milano, Milan*

Abstract

In the framework of statistical asymptotic homogenization of random fibre-reinforced composites, we propose a curved virtual element procedure that allows an exact geometric representation. We develop an approach that is able to represent exactly the involved geometry and exploits an adaptive tuning of the optimal mesh resolution through a robust and efficient residual-based a-posteriori error estimator. Furthermore, by combining such scheme and Monte Carlo simulations, a methodology is developed to determine homogenized material moduli and representative unit cell size. A gallery of numerical tests supports the proposed approach.

Keywords: Virtual element method, Curved edges, Random composite, Asymptotic homogenization, A posteriori error estimate.

1. Introduction

Composite materials are extensively used materials in many engineering applications due to their interesting properties, as, for instance, high strength-to-weight ratio and tunable features of the constituents. Use of such complex

*Corresponding author
Email address: artioli@ing.uniroma2.it (E. Artioli)

materials requires accurate yet computationally efficient methods of analysis of their mechanical response.

In reference to the scope of the present communication which focuses on *fibre reinforced* composite materials, a large number of analysis methods have been devised seeking to approximate composite structural mechanics by analyzing a representative (smaller) part of the composite microstructure, commonly called a Representative Volume Element (RVE) or Representative Unit Cell (RUC) [1, 2]. They all are based on scale decoupling leading to analyses at the local and global levels and, with some differences, apply either to doubly periodic arrangements of fibres (doubly periodic composites) or random distributions of inclusions (random composites) within a matrix medium. The local level analysis models the microstructural details to determine effective elastic properties. The composite structure is then replaced by an equivalent homogeneous material having the calculated effective properties. Such a process of calculating effective properties is usually termed *material homogenization* [3] and has led to massive interest in the scientific community since the early 70s [4, 5, 6, 7, 8, 9, 10, 11, 3].

In this regard, a significantly studied method for solving the micro scale problem is represented by *asymptotic homogenization* which can lead, in selected cases of linear elastic constituents, to closed form solution of the aforementioned problem, but, in general, requires adopting approximate numerical solutions mainly because the constituents can present nonlinear behavior and can have a random size and space distribution within the host medium. The finite element method is clearly the most utilized method to solve such a problem, and still applies to random composites requiring to solve a high number of representative unit cell problems randomly generated [12] and then to determine average material properties in a statistical sense.

In the above outlined framework, major problems involved in the micro scale computational modeling are: *i*) meshing curved objects i.e. fibre/matrix interfaces; *ii*) efficient domain discretization for any given loading condition; *iii*) computational cost due to high number of realization needed in a statistical homogenization process.

Recently, the Virtual Element Method (VEM) has been proposed and shown to be a very efficient alternative to the standard finite element method [13, 14]. It represents a generalization of the FE method with the capability of dealing with very general polygonal/polyhedral meshes. The VEM has already been successfully adopted to solve linear elasticity problems [15, 16, 17], as well as in conjunction with topology optimization and with complex material nonlinearity such as plasticity, viscoelasticity, damage and shape memory problems, see, e.g. [18, 19, 20, 21, 22, 23, 24] for a short representative list of related works. In the framework of computational homogenization, a VEM based procedure has been proposed in [25], for evaluating the antiplane shear homogenized material moduli of a doubly periodic composite material reinforced by cylindrical inclusions, more recently a study of particle-based composites via VEM has been presented in [26, 27], adopting polygonal meshes for the matrix and a single element for the inclusions. An investigation on the capability and advantages of the VEM technique in solving the micromechanical and homogenization problem for periodic composites characterized by linear mechanical response has been performed in [28].

The aim of this communication is to develop a VEM based procedure for the antiplane shear homogenization problem which tackles and solves the above mentioned issues inherent to a numerical approach for the micromechanical problem, by making use of specific features of the virtual technololgy, namely the possibility of using curvilinear polygonal elements [29, 30] (thus avoiding geometry discretization errors at fibre/matrix interface) and of using adaptive mesh refinement with hanging nodes in order to get large scale analysis on several domain realizations with a reduced computational cost. In particular, VEM elements characterized by linear and higher order polynomial approximation are proposed. Homogeneous and functionally graded constitutive laws are considered for the fibre constituents of the composite. Numerical applications are developed to assess the effectiveness of the proposed VEM elements by making several comparisons with results obtained adopting available more established techniuqes showing the advantages of the newly proposed methodology.

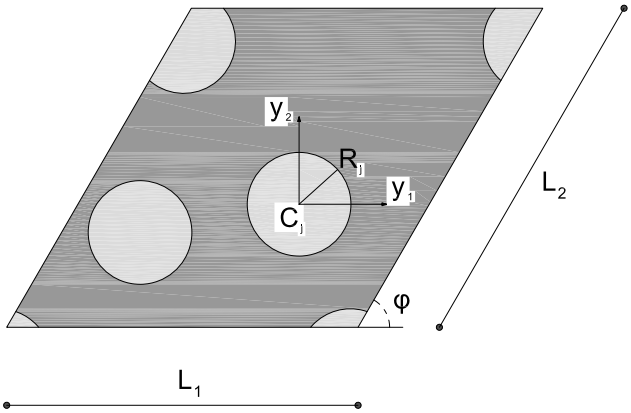

Figure 1: A stochastic realization of a parallelogram shaped repeating unit cell (RUC) of the composite with volume fraction $f = 0.2$ and three circular fibres. Geometrical parameters and fibre frame reference.

The paper is organized as follows. In Section 2 the asymptotic homogenization problem under investigation is sketched for the case of long fiber composites. In Section 3 the curvilinear VEM formulation is described. Section 4 illustrates an a posteriori error estimator for the model under investigation together with its theoretical assessment and inherent adaptive mesh refinement capability. Section 5 presents a large class of numerical tests validating the curvilinear VEM and proving the effectiveness of the proposed method as a tool for the computational homogenization of random fibre reinforced materials. Finally, conclusive remarks are given in Section 6.

2. Asymptotic homogenization of random fibre-reinforced composite

We consider a composite material, reinforced with long, parallel fibres, randomly distributed in the material with a statistically homogeneous microstructure. Fibres have circular cross section and the same radius.

At the microscale, the cross section of the composite consists of a doubly-periodic arrangement of repeating unit cells (RUC). Geometry-wise a RUC is

a parallelogram, with sides L_1, L_2, and angle φ, containing the centres of F fibres, denoted by C_j, with radii R_j, $j = 1 \dots F$, as represented in Fig. 1. In the following, we will denote $f_j = \pi R_j^2/|\mathsf{D}|$ as the volume fraction of the j^{th} fibre, and $f = \sum_{j=1}^{F} f_j$ as the total volume fraction.

In this treatment, reference will be made to effective in-plane elastic shear moduli, computed applying asymptotic homogenization. Hence, a family of equilibrium boundary value problems, indexed by a parameter $\boldsymbol{\varepsilon}$, for the longitudinal (i.e. orthogonal to fibre cross section plane) displacement field $w_{\boldsymbol{\varepsilon}}$, is considered on the composite domain:

$$\operatorname{div}(\boldsymbol{G}\nabla w_{\boldsymbol{\varepsilon}}) = 0\,, \qquad \text{in } \cup_j \Omega^{\mathrm{f}}_{j\boldsymbol{\varepsilon}} \cup \Omega^{\mathrm{m}}_{\boldsymbol{\varepsilon}}\,; \tag{1}$$

$$[\![\boldsymbol{G}\nabla w_{\boldsymbol{\varepsilon}} \cdot \boldsymbol{\nu}]\!] = 0\,, \qquad \text{on } \cup_j \Gamma_{j\boldsymbol{\varepsilon}}\,; \tag{2}$$

$$\boldsymbol{G}\nabla w_{\boldsymbol{\varepsilon}} \cdot \boldsymbol{\nu} = \frac{1}{\boldsymbol{\varepsilon}} D_j [\![w_{\boldsymbol{\varepsilon}}]\!]\,, \qquad \text{on } \cup_j \Gamma_{j\boldsymbol{\varepsilon}}\,. \tag{3}$$

where $\cup_j \Omega^{\mathrm{f}}_{j\boldsymbol{\varepsilon}}$ and $\Omega^{\mathrm{m}}_{\boldsymbol{\varepsilon}}$ denote fibres and matrix domains respectively, $\cup_j \Gamma_{j\boldsymbol{\varepsilon}}$ is the set formed by fibre/matrix interfaces, $\boldsymbol{\nu}$ is unit vector normal to $\cup_j \Gamma_{j\boldsymbol{\varepsilon}}$ pointing into $\Omega^{\mathrm{m}}_{\boldsymbol{\varepsilon}}$, and square brackets $[\![\,\cdot\,]\!]$ denote jump across the interface, defined as extra-fibre value minus intra-fibre value. In the above, the parameter $\boldsymbol{\varepsilon}$ scales the microstructure, such that $\boldsymbol{\varepsilon} = 1$ refers to the real composite material under consideration, and the homogenization limit is obtained by sending $\boldsymbol{\varepsilon}$ to zero.

Equation (1) is the field equilibrium equation; Eq. (2) represents equilibrium at the fibre/matrix interface requiring continuity of the normal-to-interface component of the shear stress; Eq. (3) is the interface constitution law.

Assuming linear elastic fibres and matrix, the relative shear moduli are given by the constitutive tensor $\boldsymbol{G}$, which respectively reads:

$$\boldsymbol{G} = \boldsymbol{G}^{\mathrm{f}}_j \quad \text{in } \Omega^{\mathrm{f}}_{j\boldsymbol{\varepsilon}}\,,\ j = 1 \dots F\,, \tag{4}$$

$$\boldsymbol{G} = \boldsymbol{G}^{\mathrm{m}} \quad \text{in } \Omega^{\mathrm{m}}_{\boldsymbol{\varepsilon}}\,. \tag{5}$$

Fibres are made of a linear elastic material with cylindrical orthotropy, their material moduli are graded along the radius, such that, setting a polar coordinate system (C_j, r_j, θ_j) for each fibre, it results:

$$\boldsymbol{G}^{\mathrm{f}}_j = (G^{\mathrm{r}}_j \boldsymbol{e}^{\mathrm{r}}_j \otimes \boldsymbol{e}^{\mathrm{r}}_j + G^{\theta}_j \boldsymbol{e}^{\theta}_j \otimes \boldsymbol{e}^{\theta}_j) g_j(\rho_j)\,, \tag{6}$$

where $\rho_j = r_j/R_j$, $g_j(\rho_j)$ is the grading function, and $(\boldsymbol{e}_j^{\mathrm{r}}, \boldsymbol{e}_j^{\theta})$ are the radial and tangential unit vectors, respectively. The matrix material is homogeneous and isotropic, so that $\boldsymbol{G}^{\mathrm{m}} = G^{\mathrm{m}}\mathbf{I}$, with $\mathbf{I}$ the second order identity tensor and G^{m} the matrix shear modulus.

Zero-thickness imperfect fibre/matrix interfaces are assumed according to the classical linear spring-layer model [11, 31, 32]. As can be deduced by Eq. (3), a linear elastic relation for the displacement jump $[\![w_{\boldsymbol{\varepsilon}}]\!]$ and the interface normal traction $\boldsymbol{G}\nabla w_{\boldsymbol{\varepsilon}} \cdot \boldsymbol{\nu}$ is assumed through the parameter D_j, with the factor $\boldsymbol{\varepsilon}^{-1}$ granting the right scaling in the homogenization limit [11].

In order to guarantee the well posedness of the above problem, the following limitations hold true:

$$G^{\mathrm{m}} > 0\,, \quad G_j^{\mathrm{r}} > 0\,, \quad G_j^{\theta} > 0\,, \quad D_j > 0\,, \quad g_j(\rho_j) > 0 \quad \text{in } (0,1]\,, \quad j = 1 \dots F. \tag{7}$$

2.1. Homogenized equilibrium equation

The asymptotic homogenization method is employed to derive the homogenized or effective constitutive tensor of the composite material. Two different length scales characterize the problem under consideration. Hence, two different space variables are introduced: the macroscopic one, x, and the microscopic one, $y = x/\boldsymbol{\varepsilon}$, $y \in \mathsf{D}$, being D the RUC (see Figure 1), whose extra-fibre space, intra-fibre space and fibre-matrix interface are denoted by D^{m}, $\mathsf{D}_j^{\mathrm{f}}$ and Γ_j, for $j = 1 \dots F$, respectively. An asymptotic expansion of the unknown displacement field is considered in the form:

$$w_{\boldsymbol{\varepsilon}}(x,y) = w_0(x,y) + \boldsymbol{\varepsilon} w_1(x,y) + \boldsymbol{\varepsilon}^2 w_2(x,y) + \dots\,, \tag{8}$$

where w_0, w_1, w_2 are D-periodic functions in y, and w_1, w_2 have null integral average over D. Substituting (8) into Problem (1)–(3) and equating the power-like terms of $\boldsymbol{\varepsilon}$, three differential problems for w_0, w_1 and w_2 are obtained, respectively, which, following a standard argument [6, 9], yield the homogenized equation for the macroscopic displacement w_0:

$$\mathrm{div}_x(\boldsymbol{G}^{\#}\nabla_x w_0) = 0\,. \tag{9}$$

Here $\nabla_x w_0$ is the macroscopic shear strain, and

$$\boldsymbol{G}^{\#} = \frac{1}{|\mathsf{D}|}\int_{\mathsf{D}} \boldsymbol{G}(\mathbf{I} - \nabla_y^{\mathrm{t}}\boldsymbol{\chi})\,\mathrm{d}a \tag{10}$$

is the effective constitutive tensor, where the superscript $^{\mathrm{t}}$ denotes the transpose, $\mathrm{d}a$ is the area element of D, $|\cdot|$ is the Lebesgue measure, and the vector-valued cell function $\boldsymbol{\chi}(y)$ has been introduced. Its components $\chi_s, s = 1, 2$, are the unique, null average, D-periodic solutions of the cell problem:

$$\mathrm{div}_y[\boldsymbol{G}(\nabla_y\chi_s - \boldsymbol{e}_s)] = 0\,, \qquad \text{in } \mathsf{D}^{\mathrm{f}} \cup \mathsf{D}^{\mathrm{m}}\,; \tag{11}$$

$$[\![\boldsymbol{G}(\nabla_y\chi_s - \boldsymbol{e}_s)\cdot\boldsymbol{\nu}]\!] = 0\,, \qquad \text{on } \cup_j\Gamma_j\,; \tag{12}$$

$$\boldsymbol{G}(\nabla_y\chi_s - \boldsymbol{e}_s)\cdot\boldsymbol{\nu} = D_j[\![\chi_s]\!]\,, \qquad \text{on } \cup_j\Gamma_j\,, \tag{13}$$

where $\boldsymbol{e}_s$ is the unit vector parallel to the y_s axis.

Using the Gauss-Green Lemma and introducing the auxiliary cell function:

$$\tilde{\boldsymbol{\chi}}(y_1, y_2) = \boldsymbol{\chi}(y_1, y_2) - (y_1\boldsymbol{e}_1 + y_2\boldsymbol{e}_2)\,, \tag{14}$$

Eq. (10) is transformed into:

$$\boldsymbol{G}^{\#} = \boldsymbol{G}^{\mathrm{m}} + \frac{1}{|\mathsf{D}|}\sum_{j=1}^{F}\int_{\mathsf{D}_j^{\mathrm{f}}}(\mathrm{div}_y\boldsymbol{G}^{\mathrm{f}})\otimes\tilde{\boldsymbol{\chi}}\,\mathrm{d}a + \frac{1}{|\mathsf{D}|}\sum_{j=1}^{F}\int_{\Gamma_j}[\![\boldsymbol{G}\boldsymbol{\nu}\otimes\tilde{\boldsymbol{\chi}}]\!]\,\mathrm{d}l\,, \tag{15}$$

where $\mathrm{d}l$ is the line element of Γ_j. Equation (15) yields the effective shear moduli of the composite material in terms of the solution $\boldsymbol{\chi}$ of the cell problem.

3. C^0 curved virtual element method

A weak formulation for the cell problem (11)-(13) is provided by the virtual work principle:

$$\begin{cases} \text{Find } \tilde{\chi}_s \in \tilde{\mathbf{V}} \text{ such that} \\ a(\tilde{\chi}_s, \delta\chi_s) = 0 \quad \forall\,\delta\chi_s \in \mathbf{V},\ s = 1, 2 \end{cases} \tag{16}$$

where $\tilde{\mathbf{V}} := H^1_{sp}(\mathsf{D})$ is the space of the admissible auxiliary cell functions $\tilde{\boldsymbol{\chi}}$ which are shift D-periodic, i.e. such that the associated $\chi_s(y_1, y_2)$ function (that is, the corresponding component s of the vector field in (14)) satisfies

$$\chi_s(y_1 + L_1, y_2) = \chi_s(y_1, y_2) = \chi_s(y_1 + L_2\cos\varphi, y_2 + L_2\sin\varphi)\,. \tag{17}$$

More precisely ($s \in \{1,2\}$)

$$\tilde{\mathbf{V}} = \Big\{ \tilde{\chi} \in L^2(\mathsf{D}) \text{ such that } \tilde{\chi}|_{\mathsf{D}_j^{\mathrm{f}}} \in H^1(\mathsf{D}_j^{\mathrm{f}}) \text{ for } j = 1,2,..,F, \\ \tilde{\chi}|_{\mathsf{D}^{\mathrm{m}}} \in H^1(\mathsf{D}^{\mathrm{m}}),\ \tilde{\chi}(y_1,y_2)+y_s \text{ satisfies (17)} \Big\}.$$

Note that, due to the last condition, the space $\tilde{\mathbf{V}}$ depends on $s \in \{1,2\}$, but we prefer to avoid expliciting such dependence in the notation. We denote by $\mathbf{V}$ the space of the admissible D-periodic variations of $\tilde{\mathbf{V}}$. The bilinear form characterizing the variational formulation is:

$$a(\tilde{\chi}_s, \delta\chi_s) = -\int_{\mathsf{D}} \mathrm{div}_y[\boldsymbol{G}(\nabla_y \tilde{\chi}_s)]\, \delta\chi_s \, \mathrm{d}\mathbf{x} \tag{18}$$

which, exploiting Gauss-Green lemma, considering constitutive equation (13) and that unit normal vectors to $\partial\mathsf{D}^{\mathrm{m}}$ on opposite sides of the unit cell are opposite, becomes:

$$\begin{aligned} a(\tilde{\chi}_s, \delta\chi_s) = &\int_{\mathsf{D}^{\mathrm{m}}} \nabla_y \delta\chi_s \cdot \boldsymbol{G}^{\mathrm{m}}(\nabla_y \tilde{\chi}_s)\mathrm{d}\mathbf{x} + \sum_{j=1}^{F} \int_{\mathsf{D}_j^{\mathrm{f}}} \nabla_y \delta\chi_s \cdot \boldsymbol{G}_j^{\mathrm{f}}(\nabla_y \tilde{\chi}_s)\mathrm{d}\mathbf{x} \\ &+ \sum_{j=1}^{F} \int_{\Gamma_j} [\![\delta\chi_s]\!]\, D_j\, [\![\tilde{\chi}_s]\!]\, \mathrm{d}l. \end{aligned} \tag{19}$$

In more compact notation, one can also write

$$a(\tilde{\chi}_s, \delta\chi_s) = \int_{\mathsf{D}} \nabla_y \delta\chi_s \cdot \boldsymbol{G}(\nabla_y \tilde{\chi}_s)\mathrm{d}\mathbf{x} + \sum_{j=1}^{F} \int_{\Gamma_j} [\![\delta\chi_s]\!]\, D_j\, [\![\tilde{\chi}_s]\!]\, \mathrm{d}l. \tag{20}$$

The form $a(\cdot,\cdot)$ is symmetric, continuous and coercive on $\tilde{\mathbf{V}}$, so that problem (16) is well posed.

3.1. The Virtual Element space

Aiming at a virtual element discretization of problem (16) with curved edges, we follow the same lines of [29]. Let $\mathcal{T}_h$ be a *simple polygonal mesh* on D, i.e. any decomposition of D in a finite set of simple polygons E, without holes and with boundary given by a finite number of edges. Whenever an element has an edge lying on an interface Γ_j, such edge is then allowed to be curved in order to describe exactly the geometry of the problem. We assume that each interface

Γ_j is parametrized by an invertible C^1 mapping γ_j from an interval in the real line into Γ_j. It is not restrictive to assume that each curved edge is a subset of only one Γ_j and therefore regular. In order to simplify the notation in the following we sometimes drop the index j, simply use Γ and

$$\boldsymbol{\gamma} \ : \ [0, L] \longrightarrow \Gamma$$

to indicate a generic curved part of the fibre/matrix interface and its associated parametrization.

In the following we will denote with e a generic edge of the mesh and with ν a generic vertex. As usual the symbol h will be associated to the diameter of objects, for instance h_E will denote the diameter of the element E and h_e the (curvilinear) length of the edge e. An h without indexes denotes as usual the maximum mesh element size.

3.2. The virtual space

In the present section we briefly review the space proposed in [29], that we will use for the discretization of the problem. As usual, we define the space element by element. Let therefore $E \in \mathcal{T}_h$. Note that E may have some curved edge, laying on some curved interface Γ_j ($j \in \{1, 2, .., F\}$). For any of such curved edges e, let $\boldsymbol{\gamma}_e : [a, b] \to e$ denote the restriction of the parametrization describing Γ_j to the edge e. Then we indicate the space of mapped polynomials (living on e) as

$$\widetilde{\mathcal{P}}_k(e) = \Big\{ p \circ \boldsymbol{\gamma}_e^{-1} \ : \ p \in \mathcal{P}_k[a, b] \Big\}.$$

The local virtual element space on E is then defined as

$$\mathbf{V}_h(E) = \Big\{ v \in H^1(E) \cap C^0(E) \ : \ v|_e \in \mathcal{P}_k(e) \text{ if } e \text{ is straight}, \\ v|_e \in \widetilde{\mathcal{P}}_k(e) \text{ if } e \text{ is curved}, -\Delta v \in \mathcal{P}_{k-2}(E) \Big\}. \tag{21}$$

The associated degrees of freedom are (see [29] for the simple proof)

- pointwise evaluation at each vertex of E;
- pointwise evaluation at $k-1$ distinct points for each edge of E;

- moments $\int_E v p_{k-2}$ for all $p_{k-2} \in \mathcal{P}_{k-2}(E)$.

As usual, the global space is obtained by a standard gluing procedure

$$\tilde{\mathbf{V}}_h = \Big\{ v \in \tilde{\mathbf{V}} \ : \ v|_E \in \mathbf{V}_h(E) \ \forall E \in \mathcal{T}_h \Big\},$$

and the same holds for the corresponding space of discrete variations

$$\mathbf{V}_h = \Big\{ v \in \mathbf{V} \ : \ v|_E \in \mathbf{V}_h(E) \ \forall E \in \mathcal{T}_h \Big\}.$$

The global degrees of freeedom are the obvious extension of the local ones. Note that on the edges of the mesh the degrees of freedom are standard Lagrange type interpolation points. Therefore, handling the discontinuities across interfaces and the periodic boundary conditions in the definition of $H^1_{sp}(\mathsf{D})$ is done exactly as in standard finite elements.

3.3. Discretization of the problem

The discretization of the problem is a combination of the scheme proposed in [25] for the case with standard straight edges and the curved-edge technology introduced in [29] for a model linear diffusion problem.

We start by introducing the following projection operator that is used to compute, on each mesh element E, an approximated gradient operator. Let $[\mathcal{P}_{k-1}(E)]^2$ denote the set of polynomial vector fields of degree $k-1$ living on E. Given $E \in \mathcal{T}_h$ and any $v_h \in \mathbf{V}_h(E)$, the operator $\Pi : \mathbf{V}_h(E) \to [\mathcal{P}_{k-1}(E)]^2$ is defined by

$$\begin{cases} \Pi(v_h) \in [\mathcal{P}_{k-1}(E)]^2 \\ \displaystyle\int_E \Pi(v_h) \cdot \mathbf{p}_{k-1} = \int_E \nabla(v_h) \cdot \mathbf{p}_{k-1} \quad \forall \mathbf{p}_{k-1} \in [\mathcal{P}_{k-1}(E)]^2 \, , \end{cases}$$

where $\nabla(v_h)$ denotes as usual the gradient of v_h (we dropped the y to simplify the notation). By definition, $\Pi(v_h)$ is the L^2 projection of ∇v_h on $[\mathcal{P}_{k-1}(E)]^2$. Note that the above operator is computable. Indeed an integration by parts shows that

$$\int_E \nabla v_h \cdot \mathbf{p}_{k-1} = -\int_E v_h (\operatorname{div} \mathbf{p}_{k-1}) \ + \ \int_{\partial E} v_h (\mathbf{p}_{k-1} \mathbf{n}_E) \, .$$

The first term on the right hand side can be computed noting that div $\mathbf{p}_{k-1}$ is a polynomial of degree $k-2$ and using the internal degrees of freedom values of v_h. The second term on the right hand side can be computed since we have complete knowledge of v_h on the boundary of E. Note that all these computations clearly require the integration of known functions on a curved element and a curved boundary; those can be accomplished as shown for instance in [33, 29, 34].

We can now describe the proposed numerical method. We start by defining the local discrete counterpart of the first bilinear form appearing in the right hand side of (20). Let $E \in \mathcal{T}_h$. We define for all $v_h, w_h \in \mathbf{V}_h(E)$ the local discrete bilinear form as

$$a_h^E(v_h, w_h) = \int_E \Pi w_h \cdot \boldsymbol{G}(\Pi v_h)\, \mathrm{d}\mathbf{x} \; + \; s^E((I-\pi)v_h, (I-\pi)w_h) \qquad (22)$$

where the first term is a direct approximation of $\int_E \nabla w_h \cdot \boldsymbol{G}(\nabla v_h)$ by substituting ∇ with Π, and the second term is the stabilization form, described below. The operator $\pi : \mathbf{V}_h(E) \to \mathcal{P}_k(E)$ can be chosen as any projection operator on polynomials of degree k, for instance one that minimizes the distance of the euclidean norm of the degree of freedom values (such particular choice has the advantage of being very simple to code, see for instance [17]). The stabilization form can be taken, for example, as

$$s^E((I-\pi)v_h, (I-\pi)w_h) = \alpha_E \sum_{i=1}^{\#dofs} \Big(\mathrm{dof}_i(w_h - \pi w_h)\Big)\Big(\mathrm{dof}_i(v_h - \pi v_h)\Big) \qquad (23)$$

where the dof_i symbol denotes evaluation at the i^{th} local degree of freedom and the positive scalar α_E is introduced in order to take into account the material constants. For example one can take $\alpha_E = \mathrm{trace}(\boldsymbol{G}(\mathbf{x}_E))/2$ with $\mathbf{x}_E$ the centroid of E or any other internal point (the method turns out to be quite robust with respect to this parameter). Note that the above stabilization, that is quite awkward to write on paper, is instead very simple to code since it is directly based on the degree of freedom values, that is what the code operates on. More details on the stabilization can be found for instance in [17].

The global discrete bilinear form is now taken as, for any v_h, w_h in $\tilde{\mathbf{V}}_h$ or

$\mathbf{V}_h$,

$$a_h(v_h, w_h) = \sum_{E \in \mathcal{T}_h} a_h^E(v_h, w_h) + \sum_{j=1}^{F} \int_{\Gamma_j} [\![w_h]\!] \, D_j \, [\![v_h]\!] \, \mathrm{d}l$$

where we observe that the jumps above can be immediately computed since the virtual functions are known explicitly on the boundaries of the elements.

The proposed Virtual Element Method then reads

$$\begin{cases} \text{Find } \tilde{\chi}_{hs} \in \tilde{\mathbf{V}}_h \text{ such that} \\ a_h(\tilde{\chi}_{hs}, \delta\chi_{hs}) = 0 \qquad \forall \delta\chi_{hs} \in \mathbf{V}_h, \ s = 1, 2. \end{cases} \tag{24}$$

To ease notation, in the following, we simply indicate either component $\chi_{hs}, \ s = 1, 2$ of the cell function with χ_h, explicitly indicating a specific component whenever needed. Note that the above construction follows the same logic and structure as for the straight-edge case [13, 25] and we refer to such papers for a more detailed description of the practical implementation of the scheme. In the code, the main difference is only the need to integrate along curved edges and on curved domains (that can be handled following the literature given above).

4. A posteriori error estimator

In the present section, inspired by [35] (see also [36]) we introduce the proposed error estimator, and develop a theoretical reliability analysis (i.e. the estimator bounds the error from above) that takes into account the material constants appearing in the problem.

We start by introducing some notation. In the following we assume for simplicity that the material tensor $\boldsymbol{G}$ is piecewise constant with respect to the mesh (see also Remark 4.1), and we define for each element $E \in \mathcal{T}_h$ the positive constants G_E^{inf}, G_E^{sup} by

$$G_E^{inf} \leq \frac{\mathbf{w} \cdot \boldsymbol{G}|_E \mathbf{w}}{\mathbf{w} \cdot \mathbf{w}} \leq G_E^{sup} \quad \forall \mathbf{w} \in \mathbb{R}^2. \tag{25}$$

Moreover for each internal edge e we define

$$G_e^{inf} := \begin{cases} \min\{G_{E^+}^{inf}, G_{E^-}^{inf}\} & \text{if } e \in \cup_j \Gamma_j \\ \max\{G_{E^+}^{inf}, G_{E^-}^{inf}\} & \text{otherwise,} \end{cases}$$

where $E^{\pm}$ represent the elements sharing e.

In order to simplify the notation, we introduce an additional assumption, which controls the jumps of $\boldsymbol{G}$ among adjacent elements of the same subdomain. Given any element E, let ω_E denote the union of all elements sharing at least a vertex with E and that lay in the same subdomain as E (either $\mathsf{D}_j^{\mathrm{f}}$ for some index j or D^{m}). Then, there exist two constants $c_\star, c^\star$ such that for all $E \in \mathcal{T}_h$ it holds

$$c_\star G_{E'}^{inf} \leq G_E^{inf} \leq c^\star G_{E'}^{inf} \qquad \forall E' \in \omega_E \ , \tag{26}$$

and the analogous for G_E^{sup}.

Given $\tilde{\chi}_h$ solution to the discrete problem (24), we introduce the following terms for the error indicator. For each $E \in \mathcal{T}_h$ we define the internal residual term

$$\eta_{R,E}^2 := \frac{h_E^2}{G_E^{inf}} \|\mathrm{div}_y[\boldsymbol{G}(\Pi\,\tilde{\chi}_h)]\|_{L^2(E)}^2.$$

For each edge e of the mesh, including the boundary and interface ones, we define the edge residual term

$$\eta_{r,e}^2 := \frac{h_e}{G_e^{inf}} \| \left[\!\left[\boldsymbol{G}(\Pi\,\tilde{\chi}_h) \cdot \boldsymbol{\nu}_e\right]\!\right] \|_{L^2(e)}^2.$$

For each edge e on the interface Γ we also consider the interface residual term

$$\eta_{\Gamma,e}^2 := \frac{h_e}{G_e^{inf}} \| \left\{\boldsymbol{G}(\Pi\,\tilde{\chi}_h) \cdot \boldsymbol{\nu}_e\right\} - D[\![\chi_h]\!] \|_{L^2(e)}^2,$$

where the $\{...\}$ symbol above denotes the average operator among the left and right elements sharing the edge e. Furthermore, for each element $E \in \mathcal{T}_h$ we consider the additional term taking into account the inconsistency stemming from the VEM formulation

$$\eta_{S,E}^2 := s^E((I-\pi)\tilde{\chi}_h, (I-\pi)\tilde{\chi}_h).$$

Finally, the local and global error estimators are

$$\eta_E^2 = \eta_{R,E}^2 + \eta_{S,E}^2 + \frac{1}{2}\sum_{e\in\partial E} \eta_{r,e}^2 + \frac{1}{2}\sum_{e\in\partial E\cap\Gamma} \eta_{\Gamma,e}^2 \qquad \forall E \in \mathcal{T}_h, \tag{27}$$

$$\eta^2 = \sum_{E\in\mathcal{T}_h} \eta_E^2. \tag{28}$$

In the following we assume that the operator π in (23) is continuous in the H^1 norm, a property that holds for essentially all choices used in the literature. In order to state the reliability result we require the following mesh assumptions, that are standard in the VEM literature.

Mesh assumptions. There exists a positive constant ρ such that all elements E of the mesh family $\{\mathcal{T}_h\}_h$ are star-shaped with respect to a ball with radius $R_E \geq \rho h_E$. Moreover all edges e of each element E of the mesh family $\{\mathcal{T}_h\}_h$ have length $h_e \geq \rho h_E$.

Theorem 4.1. *Let the mesh assumptions above hold. Then it exists a uniform constant C, independent of the mesh and the material constants, such that the error $\tilde{\chi} - \tilde{\chi}_h$ satisfies*

$$a(\tilde{\chi} - \tilde{\chi}_h, \tilde{\chi} - \tilde{\chi}_h) \leq C\, \eta^2.$$

Proof. In the following the symbol $\lesssim$ will denote a bound up to a constant that is independent of the mesh and the material constants. We note that the constant $\alpha_E = \text{trace}(\boldsymbol{G}(x_E))/2$ proposed for the stabilization term in (23) is equivalent (up to universal constants) to G_E^{sup} . Therefore, assuming to use stabilization (23) and recalling standard results in the VEM literature, we have for all elements E and all v_h in the discrete space

$$G_E^{sup} \|\nabla(I-\pi)v_h\|^2_{L^2(E)} \lesssim s^E((I-\pi)v_h,(I-\pi)v_h) \lesssim G_E^{sup} \|\nabla(I-\pi)v_h\|^2_{L^2(E)}. \tag{29}$$

Let the error $\varphi = \tilde{\chi} - \tilde{\chi}_h \in \mathbf{V}$ and let $\varphi_I \in \mathbf{V}_h$ be an interpolant of φ to be better defined later. First using the continuous equation (16), then adding/subtracting φ_I and using (24), we obtain

$$\begin{aligned} a(\tilde{\chi} - \tilde{\chi}_h, \tilde{\chi} - \tilde{\chi}_h) &= a(\tilde{\chi} - \tilde{\chi}_h, \varphi) = -a(\tilde{\chi}_h, \varphi) = -a(\tilde{\chi}_h, \varphi - \varphi_I) - a(\tilde{\chi}_h, \varphi_I) \\ &= -a(\tilde{\chi}_h, \varphi - \varphi_I) - a(\tilde{\chi}_h, \varphi_I) + a_h(\tilde{\chi}_h, \varphi_I). \end{aligned} \tag{30}$$

By recalling that $\Pi\tilde{\chi}_h$ is the L^2 projection of $\nabla\tilde{\chi}_h$ on $[\mathcal{P}_{k-1}(E)]^2$ and noting that $\nabla\pi\tilde{\chi}_h \in [\mathcal{P}_{k-1}(E)]^2$, we can derive the following preliminary bounds for

for all elements E

$$\|\boldsymbol{G}^{1/2}(\nabla\tilde{\chi}_h - \Pi\tilde{\chi}_h)\|^2_{L^2(E)} \leq G_E^{sup}\|\nabla\tilde{\chi}_h - \Pi\tilde{\chi}_h\|^2_{L^2(E)}$$
$$\leq G_E^{sup}\|\nabla\tilde{\chi}_h - \nabla\pi\tilde{\chi}_h\|^2_{L^2(E)} \lesssim s^E((I-\pi)\tilde{\chi}_h, ((I-\pi)\tilde{\chi}_h), \qquad (31)$$

where we used (29). Let us observe that it holds

$$\begin{aligned} a(\tilde{\chi}_h, \varphi - \varphi_I) &= \sum_{E\in\mathcal{T}_h}\int_E (\nabla\tilde{\chi}_h - \Pi\tilde{\chi}_h)\cdot\boldsymbol{G}\nabla(\varphi-\varphi_I)\mathrm{d}\mathbf{x} \\ &\quad + \sum_{E\in\mathcal{T}_h}\int_E \Pi\tilde{\chi}_h\cdot\boldsymbol{G}\nabla(\varphi-\varphi_I)\mathrm{d}\mathbf{x} + \sum_{j=1}^F\int_{\Gamma_j}[\![\tilde{\chi}_h]\!]D_j[\![\varphi-\varphi_I]\!]dl \\ &= \sum_{E\in\mathcal{T}_h}(I_E + II_E) + \sum_{j=1}^F\int_{\Gamma_j}[\![\tilde{\chi}_h]\!]D_j[\![\varphi-\varphi_I]\!]dl. \end{aligned}$$

Employing the Cauchy-Schwarz inequality, (25) and (31) we obtain

$$\sum_{E\in\mathcal{T}_h} I_E \lesssim \left(\sum_{E\in\mathcal{T}_h} s^E((I-\pi)\tilde{\chi}_h, (I-\pi)\tilde{\chi}_h)\right)^{1/2}\left(\sum_{E\in\mathcal{T}_h} G_E^{sup}\|\nabla(\varphi-\varphi_I)\|^2_{L^2(E)}\right)^{1/2}.$$

Moreover, integration by parts yields

$$\begin{aligned} \sum_{E\in\mathcal{T}_h} II_E &= -\sum_{E\in\mathcal{T}_h}\int_E \nabla\cdot(\boldsymbol{G}\Pi\tilde{\chi}_h)(\varphi-\varphi_I)\mathrm{d}\mathbf{x} - \sum_{e\in\mathcal{E}_h}\int_e [\![\boldsymbol{G}\Pi\tilde{\chi}_h\cdot\boldsymbol{\nu}_e]\!]\{\varphi-\varphi_I\}dl \\ &\quad -\sum_{j=1}^F\sum_{e\in\Gamma_j}\int_e\{\boldsymbol{G}\Pi\tilde{\chi}_h\cdot\boldsymbol{\nu}_e\}[\![\varphi-\varphi_I]\!]. \end{aligned}$$

Secondly, first recalling the definition of Π and that $\boldsymbol{G}|_E$ is constant, then using again (31) and standard properties of symmetric bilinear forms we have

$$\begin{aligned} a_h(\tilde{\chi}_h, \varphi_I) - a(\tilde{\chi}_h, \varphi_I) &= \sum_{E\in\mathcal{T}_h}\left(\int_E(\Pi\tilde{\chi}_h - \nabla\tilde{\chi}_h)\cdot\boldsymbol{G}\nabla\varphi_I\mathrm{d}\mathbf{x} + s^E((I-\pi)\tilde{\chi}_h, (I-\pi)\varphi_I)\right) \\ &\lesssim \Big(\sum_{E\in\mathcal{T}_h} s^E((I-\pi)\tilde{\chi}_h, (I-\pi)\tilde{\chi}_h)\Big)^{1/2}\Big(\sum_{E\in\mathcal{T}_h}\|\boldsymbol{G}^{1/2}\nabla\varphi_I\|^2_{L^2(E)} \\ &\quad + s^E((I-\pi)\varphi_I, (I-\pi)\varphi_I)\Big)^{1/2}. \end{aligned}$$

We now observe that (31) and the continuity of the operator π in H^1 yield

$$s^E((I-\pi)\varphi_I, (I-\pi)\varphi_I) \lesssim G_E^{sup}\|\nabla(I-\pi)\varphi_I\|^2_{L^2(E)} \lesssim G_E^{sup}\|\nabla\varphi_I\|^2_{L^2(E)}. \quad (32)$$

Collecting the above terms in (30), we obtain

$$
\begin{aligned}
a(\varphi,\varphi) \quad \lesssim \quad & \left(\sum_{E\in\mathcal{T}_h} s^E((I-\pi)\tilde{\chi}_h,(I-\pi)\tilde{\chi}_h\right)^{1/2}\left(\sum_{E\in\mathcal{T}_h} G_E^{sup}\|\nabla(\varphi-\varphi_I)\|^2_{L^2(E)}\right)^{1/2} \\
& + \sum_{j=1}^{F}\sum_{e\in\Gamma_j}\|\{\boldsymbol{G}\Pi\tilde{\chi}_h\cdot\boldsymbol{\nu}_e\}-D_j[\![\tilde{\chi}_h]\!]\|_{L^2(e)}\|[\![\varphi-\varphi_I]\!]\|_{L^2(e)} \\
& + \sum_{E\in\mathcal{T}_h}\|\nabla\cdot(\boldsymbol{G}\Pi\tilde{\chi}_h)\|_{L^2(E)}\|\varphi-\varphi_I\|_{L^2(E)} \\
& + \sum_{e\in\mathcal{E}_h}\|[\![\boldsymbol{G}\Pi\tilde{\chi}_h\cdot\boldsymbol{\nu}_e]\!]\|_{L^2(e)}\|\{\varphi-\varphi_I\}\|_{L^2(e)} \\
& + \left(\sum_{E\in\mathcal{T}_h} s^E((I-\pi)\tilde{\chi}_h,(I-\pi)\tilde{\chi}_h)\right)^{1/2}\left(\sum_{E\in\mathcal{T}_h} G_E^{sup}\|\nabla\varphi_I\|^2_{L^2(E)}\right)^{1/2} \qquad (33)
\end{aligned}
$$

We now select $\varphi_I \in \mathbf{V}_h$ (that we define piecewise on each $\mathsf{D}_j^{\mathrm{f}}$ or D^{m} and therefore may have jumps across the subdomains) as the Clément-type interpolant operator for the Virtual Elements introduced in [37], here extended in trivial way to the case with curved edges. By combining the theoretical results in [37] with those derived in [29] for curved edges, one can obtain the following approximation results for all elements E (and $e \in \partial E$)

$$
\begin{aligned}
&\|\varphi-\varphi_I\|_{L^2(E)} \lesssim h_E\|\nabla\varphi\|_{L^2(\omega_E)} \\
&\|\nabla\varphi_I\|_{L^2(E)} \leq \|\nabla\varphi\|_{L^2(\omega_E)} \\
&\|(\varphi-\varphi_I)|_E\|_{L^2(e)} \lesssim h_E^{1/2}\|\nabla\varphi\|_{L^2(\omega_E)}
\end{aligned}
\qquad (34)
$$

where ω_E denotes the union of all elements sharing at least a vertex with E and that lay in the same subdomain as E (either $\mathsf{D}_j^{\mathrm{f}}$ for some index j or D^{m}).

Employing in (33) the above bounds together with standard trace inequalities, (25) and assumption (26) yields the thesis:

$$
\begin{aligned}
a(\varphi,\varphi) \quad \lesssim \quad & \sum_{E\in\mathcal{T}_h} \frac{h_E^2}{G_E^{inf}} \|\nabla\cdot(\boldsymbol{G}\Pi\tilde{\chi}_h)\|^2_{L^2(E)} \\
& + \sum_{e\in\mathcal{E}_h} \frac{h_e}{G_e^{inf}} \|[\![\boldsymbol{G}\Pi\tilde{\chi}_h\cdot\boldsymbol{\nu}_e]\!]\|^2_{L^2(e)} \\
& + \sum_{j=1}^{F}\sum_{e\in F_j} \frac{h_e}{G_e^{inf}} \|\{\boldsymbol{G}\Pi\tilde{\chi}_h\cdot\boldsymbol{\nu}_e\} - D_j[\![\tilde{\chi}_h]\!]\|^2_{L^2(e)} \\
& + \max_{E\in\mathcal{T}_h}(G_E^{sup}/G_E^{inf}) \sum_{E\in\mathcal{T}_h} s^E((I-\pi)\tilde{\chi}_h,(I-\pi)\tilde{\chi}_h.
\end{aligned}
$$

Remark 4.1. *The assumption on the material tensor, i.e.* $\mathbf{G}$ *piecewise constant with respect to the mesh, can be relaxed. For instance, Theorem 4.1 is still valid with the same expression for the a posteriori error indicator* η *if we suppose that* $\mathbf{G}$ *is a smooth function on the computational mesh. However, suitable quadrature formulas have to be employed in order to practically compute the internal, boundary and interface residual terms. Moreover, the efficiency of the error indicators requires to control the so-called oscillation terms measuring the polynomial approximation of the tensor* $\mathbf{G}$ *[38].*

4.1. Adaptive mesh refinement algorithm based on a-posteriori error estimator

This section is devoted to describing how the above a-posteriori error estimate can be employed to drive an adaptive mesh refinement procedure. As detailed in the following section, adaptivity represents a crucial tool to efficiently compute overall elastic properties for random fibre reinforced composites. As already done with a similar algorithm, e.g., in [39, 40], we here devise an algorithm based on the classical paradigm (see, e.g., [41] and the references therein)

$$
\texttt{SOLVE} \rightarrow \texttt{ESTIMATE} \rightarrow \texttt{MARK} \rightarrow \texttt{REFINE}
$$

staggered along the following steps. Given an initial (relatively coarse) representative unit cell mesh on which a solution has been computed:

- compute local element error indicators (see Eq. (27));
- sort elements with respect to local error indicator;
- mark elements according to the so-called Dörfler marking strategy, i.e. starting from the local largest error indicator and proceeding in a decreasing order mark the corresponding elements until a fixed percentage (here we employ 40 %) of the global error indicator η is reached.
- refine marked elements adopting centroid-edge midpoint ray algorithm [39, 40];
- compute a new solution for the refined mesh;
- iterate until a certain threshold for the global error is reached.

5. Numerical tests

This section presents numerical tests on the proposed VEM based strategy for the homogenization of fibre-reinforced composite materials. In particular, in Section 5.1 we numerically explore the accuracy and convergence properties of the curved virtual element method for the asymptotic homogenization in the basic case of doubly periodic composite materials adopting uniform mesh refinement. In Section 5.2, we apply the mesh refinement algorithm of Section 4.1 to investigate the capability of our a posteriori error estimate to drive an effective adaptive procedure. Last, in Section 5.3 we address statistical homogenization of composite materials with randomly distributed fibres by joint application of the adaptive mesh refinement strategy and Monte Carlo simulations.

5.1. Validation and accuracy of curved virtual element technology: doubly periodic functionally graded fibre reinforced composite

For accuracy and convergence assessment, we here study doubly periodic fibre reinforced composites for different fibre arrangements and material setups. A given doubly periodic composite unit cell is identified through the usual dimensionless geometrical parameters φ, $\kappa = L_2/L_1$, $f = \pi R^2/|\mathsf{D}|$ (being R the

radius of the single circular fibre embedded into the RUC), and the following ones for material properties:

- fibre/matrix stiffness ratio (contrast factor) $\xi = G^{\mathrm{r}}/G^{\mathrm{m}}$;
- grading intensity factor $\omega = g(0)/g(1)$;
- dimensionless interface parameter $\delta = D/(G^{\mathrm{m}}L_1)$;
- $\sigma^2 = G^{\theta}/G^{\mathrm{r}}$.

The simulations refer to isotropic exponentially-graded fibres, with $g(\rho) = \exp(-\lambda\rho)$, and $\sigma = 1$, so that $g(0) = 1$, and $G^{\mathrm{r}} = G^{\theta}$ represents the shear modulus at fibre axis. We present results corresponding to three types of mesh discretizations, namely triangles, Voronoi polygons, quadrilaterals, indicated in the sequel as Tri-mesh, Poly-mesh, Quad-mesh, respectively. Representative meshes for square (resp. parallelogram) unit cell are portrayed in Fig. 2 with the three types of adopted discretizations. Presented results are obtained for order $k = 2, 3, 4$, respectively. As reference results we use the analytical method provided in [42] selecting a high number of terms in the series expansion for the unknown cell function in order to have high accuracy.

In Figure 3 we report $h-$convergence plots for the cell function $\boldsymbol{\chi}(y)$ in the H^1-error norm for uniform mesh refinement, for a set of cases selected as the more significant ones over an extensive test campaign.

Since the exact solution is piecewise regular in each subdomain and we have an exact geometric representation of the interface, the expected convergence rate is $O(h^k)$ (see [29]) which is obtained for all examined material patterns and any given order k. We notice that quadrilateral elements produce slightly more accurate results among the three compared discretizations. From a standpoint of material setup effect on overall accuracy, it is observed that skew unit cells as well as non-homogeneous fibres require higher computational cost to reach a given accuracy level with respect to homogeneous fibres lodged into a square lattice. As a further proof of the efficiency of a curved element approach for the problem under investigation, in Fig. 4 we plot the case of square lattice

with graded fibres and straight-edge quadratic polygons across the fibre/matrix interface, thus introducing a rectification error on such interior boundary. A sub-optimal convergence rate for all three discretizations is expected due to this geometric inconsistency [29] (see also [43] for FEM) and can be clearly observed.

5.2. Adaptive mesh refinement procedure: doubly periodic functionally graded fibre reinforced composite

In order to validate the proposed a-posteriori error estimator we apply the adaptive mesh refinement algorithm (cf. Section 4.1) to the homogenization problem of fibre reinforced doubly periodic composites introduced in the previous section. The analysis focuses on square fibre arrangements for simplicity. We present results corresponding to quadrilateral and Voronoi polygonal discretizations, obtained for order $k = 2, 3$, respectively. Reference solutions are derived resorting to the analytical method proposed in [42].

In Figure 5 we report $\#dof-$convergence plots for the cell function components χ_h in the H^1-error norm, for a set of selected fibre grading cases corresponding to isotropic homogeneous fibres with exponential grading and fibre volume fractions $f = 0.4, 0.6$. Efficiency and reliability of the proposed error estimator is clearly observed as the error curves for the adaptive mesh refinement solutions present the optimal slopes $O((\#dofs)^{-k/2})$ for given k and grant significantly lower error levels if compared with homologous (i.e. with the same number $\#dofs$ of degrees of freedom) uniform mesh refinement solutions.

In Figure 6, for illustrative purposes, we report the cases of a homogeneous (resp. a graded composite) with different volume fractions and the relative meshes at different adaptive mesh refinement iterations. The refinement process clearly shows localization of the error depending on the unit cell components and, in particular, in the vicinity of the unit cell fibre/matrix interface, and of the exterior boundary edges along the direction of each Cartesian component of the unit cell function, with more error spreading within the fibre domain in the graded case. These are in fact the areas characterized by the steepest gradient for any of the two unknown field components χ_h.

From the above numerical evidence, it can be inferred that for the relevant case of random composites, where a statistical homogenization approach imply solving for possibly large number of RUC random realizations, the above tool may be utilized as a means of tuning a *computationally efficient* mesh for actual solution of the cell problem at a lower computational cost than using a standard uniformly refined mesh. This point is addressed in the following section.

5.3. Statistical homogenization of random composites

The present section is devoted to the application of the proposed and validated adaptive mesh refinement strategy to the crucial issue of numerical estimation of the RUC size for random lattices, assuming statistically homogeneous microstructures, yielding an isotropic effective behaviour.

In this view, a quantitative estimation of the RUC size plays an important role from accuracy and computational efficiency standpoints, since the effective modulus $G^{\#}$, obtained by Eq. (15) is a random variable depending on the specific realization of the RUC D. [1] For homogenization purposes, the RUC size is determined in order to ensure a given relative accuracy ϵ of $G^{\#}$. Based on statistical arguments, in order to avoid use of large RUCs requiring heavy computational effort, use of smaller RUCs might be compensated by averaging over higher numbers of realizations of the microstructure to get a prefixed accuracy [44]. Indeed, recalling that the width of the 95% confidence interval is twice the standard deviation $\sigma_{G^{\#}}$ of $G^{\#}$, i.e. $2\sigma_{G^{\#}}/\mu_{G^{\#}} \leq \epsilon$, where $\mu_{G^{\#}}$ denotes the mean value, the standard deviation of $G^{\#}$ resulting from n independent realizations D is given by $\sigma^n_{G^{\#}} = \sigma_{G^{\#}}/\sqrt{n}$, so that n could be chosen according to

$$n \geq 4\,\mathrm{CV}^2_{G^{\#}}/\epsilon^2\,, \tag{35}$$

where $\mathrm{CV}_{G^{\#}} = \sigma_{G^{\#}}/\mu_{G^{\#}}$ is the coefficient of variation.

[1] If the RUC were a representative volume element (RVE), the dispersion of $G^{\#}$ would theoretically vanish.

The idea is then to solve any of these n realizations, for a given RUC size, using the effective adaptive mesh refinement procedure previously developed and compare with a standard uniform mesh refinement strategy, for the relevant case under consideration where a large number of material domain realizations are needed in order to reach a desired accuracy on the overall material quantities.

To do so, for any given RUC domain realization taken into account in a Monte Carlo simulation (which indeed requires to be meshed and solved), with the aim of comparing computational costs of the two procedures, starting from one initial coarse mesh, we perform a preliminary mesh discretization, adopting, respectively, uniform and adaptive mesh refinement, pursuing a global error level (cf. Eq. (28) and Fig. 5) lower than a prescribed threshold, fixed in 10^{-3} for the current analysis. We then perform Monte Carlo simulations with the two mesh families, comparing accuracy and efficiency of the two approaches.

In the following, we consider square RUCs with equal, isotropic, exponentially-graded fibres with volume fraction $f = 0.4$, 0.6, stiffness ratio $\xi = 500$, $\omega = 8$, $\delta \to \infty$. The RUC side-to-fibre diameter ratio S ranges from 3.96 to 15.85, meaning that the number of fibres included into a RUC ranges from 8 to 128.

Fig. 7 shows the normalized mean value $\mu_{G^\#}/\mathsf{G}^m$ and the dispersion of $G^\#$ as a function of the RUC size resulting from $k = 2$, quadrilateral and Voronoi discretizations, obtained with the two meshing strategies. In terms of accuracy, both discretizations seem to converge and it is observed that even a square RUC with $S \geq 8$ (hence, comprising at least 32 fibres) can be used to obtain a fair estimate of $\mu_{G^\#}$ in the present case. Table 1 shows the coefficient of variation $\mathrm{CV}_{G^\#}$ as a function of the RUC size for the two approaches, together with the ratio between the computational cost of the adaptive mesh refinement (A.M.R.) solution and the uniform mesh refinement (U.M.R.) as a function of RUC size, referring only to the actual computational time of the steps involved in solving the cell problem and computing the effective modulus for the whole realizations examined for a given value S (i.e. without taking into account the computational cost of pre-tuning the mesh).

6. Conclusion

In this work we proposed an adaptive curvilinear Virtual Element method of higher order for the asymptotic homogenization of random fibre-reinforced composite materials. The presented approach is based on an a-posteriori error estimator which can drive adaptive mesh refinement of the representative unit cell domain to be studied for a given material setup. Both the curvilinear virtual element technology and the adaptive mesh refinement procedure have been validated on a number of numerical benchmarks taking into account various microstructure configurations. In application to the relevant case of randomly distributed fibres within the composite, following a statistical approach, the aforementioned procedure has been shown to grant accurate and cost-effective homogenized quantities with respect to the standard uniform mesh refinement results.

Acknowledgements

E. Artioli gratefully acknowledges the partial financial support of PRIN 2017 project "3D PRINTING: A BRIDGE TO THE FUTURE (3DP_Future). Computational methods, innovative applications, experimental validations of new materials and technologies.", grant 2017L7X3CS_004.

L. Beirão da Veiga and M. Verani have been partially supported by MIUR through the PRIN grant n. 201744KLJL and by INdAM-GNCS.

L. Beirão da Veiga was also partially supported by the European Research Council through the H2020 Consolidator Grant (grant no. 681162) CAVE, Challenges and Advancements in Virtual Elements. This support is gratefully acknowledged.

RUC size	S_1	S_2	S_3	S_4	S_5
			$\mathrm{CV}_{G^\#}$ - $f = 0.4$ - Quad		
U.M.R.	0.053	0.050	0.037	0.026	0.015
A.M.R.	0.065	0.055	0.039	0.028	0.018
			comp. cost ratio (A.M.R./U.M.R.)		
	79.4%	75.2%	70.5%	66.8%	61.3%
			$\mathrm{CV}_{G^\#}$ - $f = 0.6$ - Poly		
U.M.R.	0.049	0.046	0.033	0.023	0.016
A.M.R.	0.073	0.059	0.039	0.024	0.015
			comp. cost ratio (A.M.R./U.M.R.)		
	88.1%	85.2%	79.5%	72.9%	67.3%

Table 1: Statistical homogenization of random composites: determination of RUC size for random graded composites, $f = 0.4$ (quadrilateral), $f = 0.6$ (Voronoi), for $k = 2$. Coefficient of variation and computational cost ratio of adaptive *vs.* uniform mesh refinement strategies as function of the RUC size.

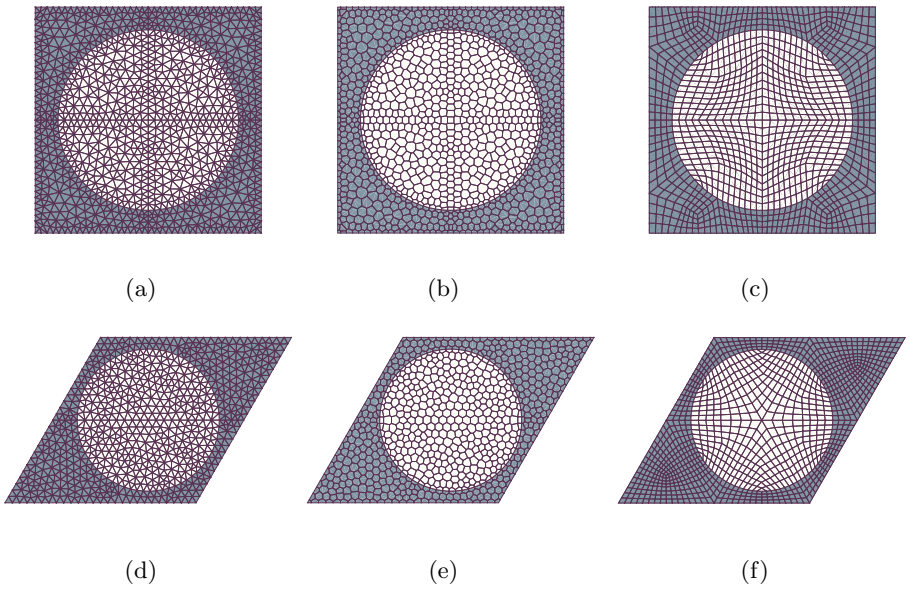

Figure 2: Doubly periodic composite. Representative unit cell meshes. Upper row: square lattice; lower row: parallelogram lattice. Circular fibre inclusion with volume fraction $f = 0.5$. (a)-(d) Tri-mesh. (b)-(e) Poly-mesh. (c)-(f) Quad-mesh.

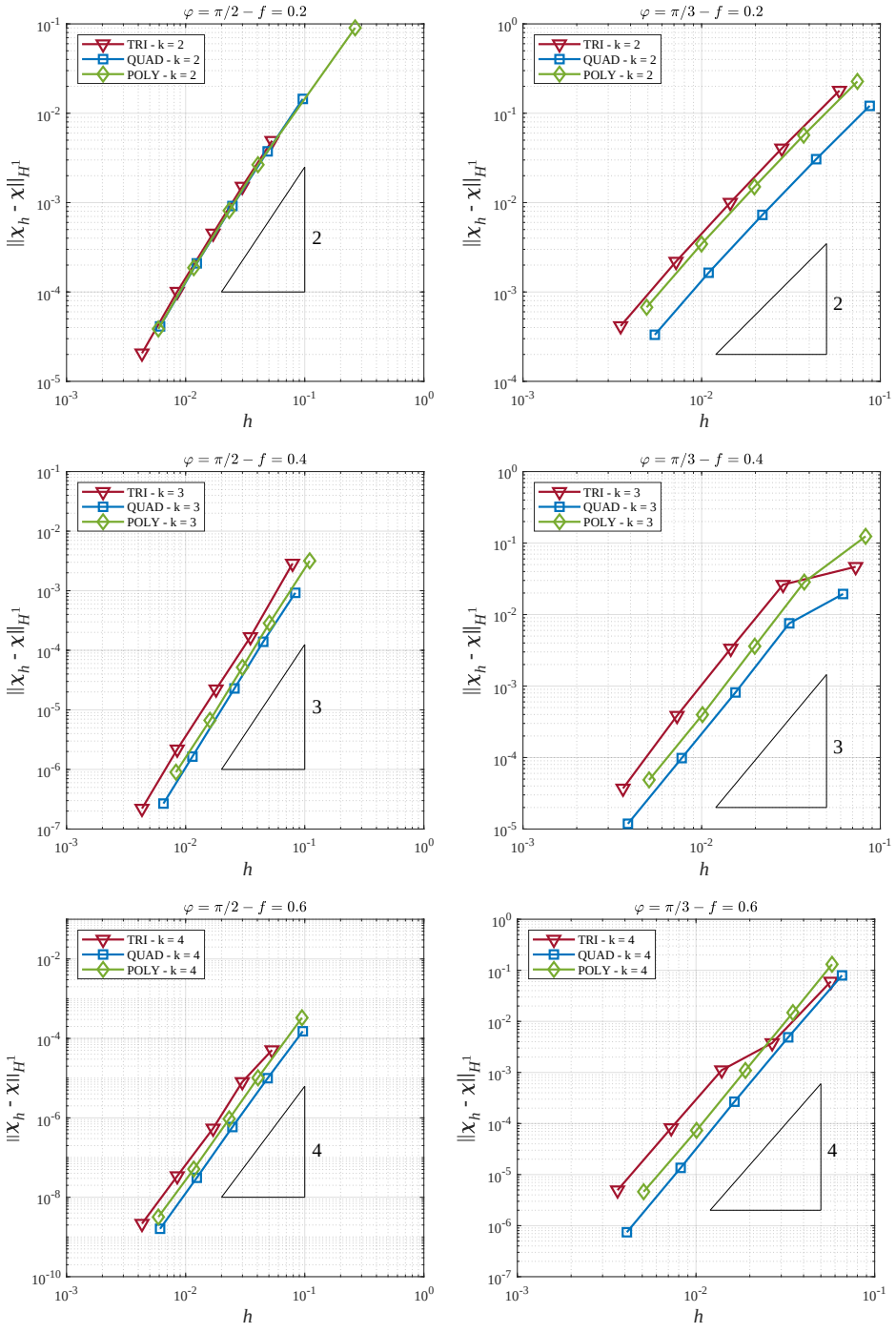

Figure 3: Doubly periodic composites, with $f = 0.2,\ 0.4,0.6$. $h-$convergence plots for $k = 2, 3, 4$, for the cell function $\boldsymbol{\chi}(y)$ in the H^1-error norm for uniform mesh refinement. Left column: square lattice, isotropic homogeneous fibres: $\delta =\!\!\rightarrow \infty$, $\xi = 500$. Right column: parallelogram lattice, isotropic exponentially graded fibres: $\xi = 500$, $\omega = 8$, $\delta = 10$.

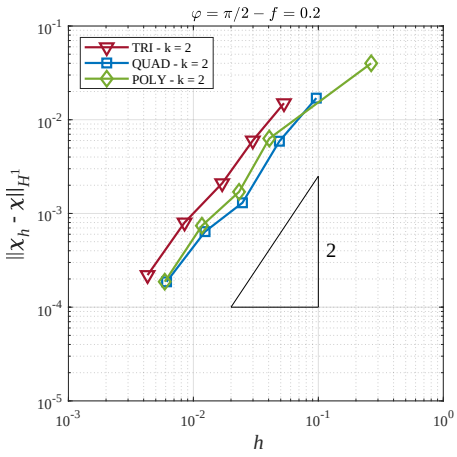

Figure 4: Doubly periodic composite. Sub-optimal $h-$convergence plots for $k = 2$, for the cell function $\boldsymbol{\chi}(y)$ in the H^1-error norm for uniform mesh refinement and *rectified* fibre/matrix interface. Square lattice, isotropic homogeneous fibres: $\xi = 500$, $\delta =\rightarrow \infty$.

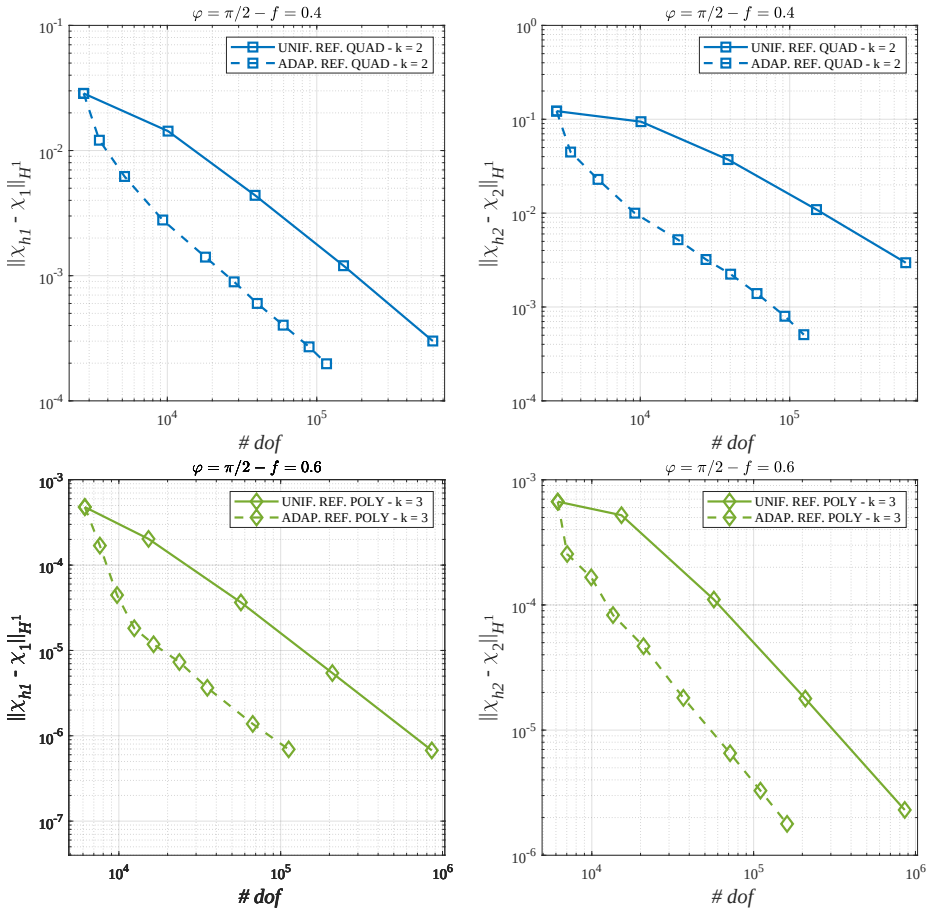

Figure 5: Doubly periodic composite. $\#\ dof-$convergence plots for $k = 2, 3$, for the cell function components χ_s $(s = 1, 2)$ in the H^1-error norm for uniform *vs.* adaptive mesh refinement: square lattice, imperfect interfaces with $\delta = 10$. Left column: isotropic homogeneous fibres with $\xi = 500$. Right column: isotropic exponentially graded fibres with $\xi = 500$, $\omega = 8$, $\delta = 10$. Upper row: $f = 0.4$, $k = 2$. Lower row: $f = 0.6$, $k = 3$.

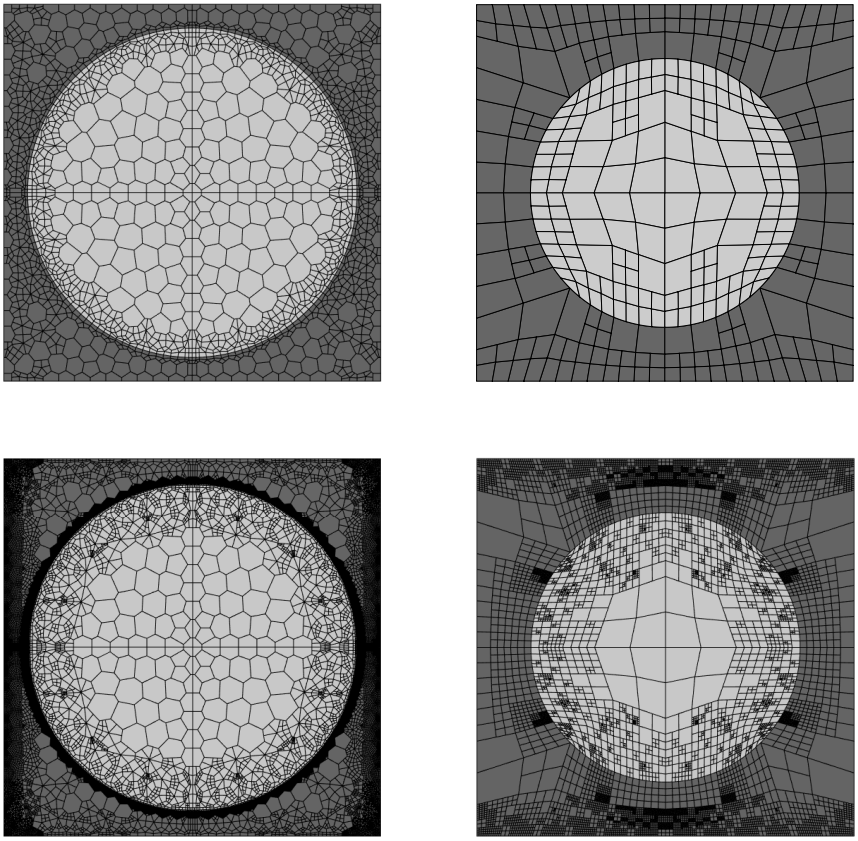

Figure 6: Adaptive mesh refinement strategy for the cell function components χ_s, $s = 1$-left column, $s = 2$-right column. Square lattice, interfaces with $\delta = 10$. Left column: isotropic homogeneous fibres with $\xi = 500$, $f = 0.6$, $k = 2$ with Voronoi discretization. Right column: isotropic exponentially graded fibres with $\xi = 500$, $\omega = 8$, $\delta = 10$, $f = 0.2$, $k = 3$ with quadrilateral discretization. Upper row: $2-nd$ refinement iteration. Lower row: $6-th$ refinement iteration.

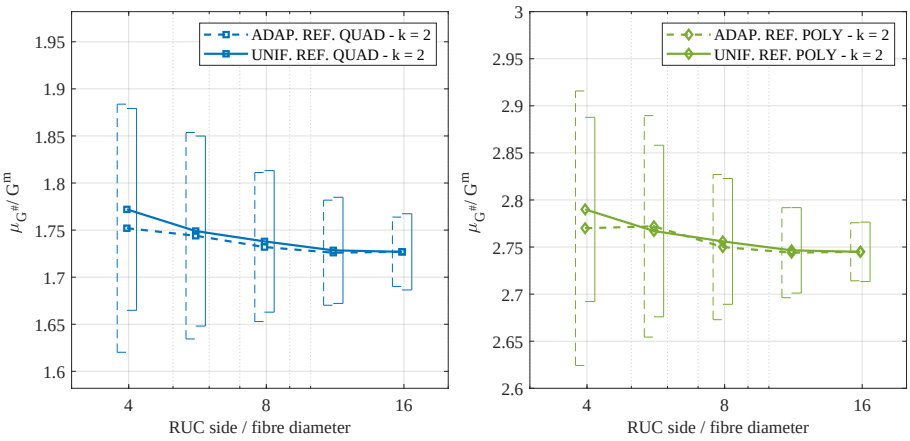

Figure 7: Statistical homogenization of random composites: determination of RUC size for random graded composites, $f = 0.4$ (quadrilateral - left), $f = 0.6$ (Voronoi - right), for $k = 2$. Normalized mean value $\mu_{G^\#}/\mathsf{G}^m$ and dispersion of $G^\#$, comparing adaptive *vs.* uniform mesh refinement strategies as function of the RUC size.

[1] R. Hill, Elastic properties of reinforced solids: some theoretical pnnciples, J. Mech. Phys. Solids 11 (1963) 357–372.

[2] Z. Hashin, Analysis of composite materials–a survey, J. Appl. Mech. 50 (1983) 481–505.

[3] P. Suquet, Elements of homogenization theory for inelastic solid mechanics, in: E. Sanchez-Palencia, A. Zaoui (Eds.), Homogenizat!on techniques for composite media, Springer, Berlin, Heidelberg, New York, 1987, pp. 194–278.

[4] E. Larsen, Neutron transport and diffusion in inhomogeneous media, Int. J. Math. Phys. 16 (1975) 1421–1427.

[5] E. Sanchez-Palencia, Comportements local et macroscopique d'un type de milieux physiques heterogenes, Int. J. Eng. Sci. 12 (1974) 331–351.

[6] A. Bensoussan, J. Lions, G. Papanicolau, Asymptotic Analysis for Periodic Structures, North-Holland, Amsterdam, 1978.

[7] G. Duvaut, Homogeneization et materiaux composite, in: P. Ciarlet, M. Rouseau (Eds.), Theoretical and AppliedMechanics, North-Holland, Amsterdam, 1976, pp. 194–278.

[8] J. Lions, Asymptotic expansions in perforated media with a periodic structure, Rocky Mountain J. Math. 10 (1980) 125–140.

[9] E. Sanchez-Palencia, Non-Homogeneous Media and Vibration Theory, Lecture notes in physics, Springer, Berlin, 1980.

[10] J. Lions, Some methods in the Mathematical Analysls Analysis of Systems and their Control, Gordon and Breach Science Publishers, New York, 1981.

[11] F. Lene, D. Leguillon, Homogenized constitutive law for a partially cohesive composite material, Int. J. Solids Struct. 18 (1982) 443–458.

[12] D. Joyce, W. J. Parnell, A. R. C., I. D. Abrahams, An integral equation method for the homogenization of unidirectional fibre-reinforced media; antiplane elasticity and other potential problems, Proc. R. Soc. A 473 (2017) 20170080.

[13] L. Beirão da Veiga, F. Brezzi, L. D. Marini, A. Russo, The hitchhiker's guide to the virtual element method, Math. Models Methods Appl. Sci. 24 (08) (2014) 1541–1573.

[14] L. Beirão da Veiga, F. Brezzi, A. Cangiani, G. Manzini, L. D. Marini, A. Russo, Basic principles of virtual element methods, Math. Models Methods Appl. Sci. 23 (1) (2013) 199–214.

[15] L. Beirão da Veiga, F. Brezzi, L. D. Marini, Virtual elements for linear elasticity problems, SIAM J. Numer. Anal. 51 (2) (2013) 794–812.

[16] A. L. Gain, C. Talischi, G. H. Paulino, On the virtual element method for three-dimensional linear elasticity problems on arbitrary polyhedral meshes, Comput. Methods Appl. Mech. Engrg. 282 (2014) 132–160.

[17] E. Artioli, L. Beirão da Veiga, C. Lovadina, E. Sacco, Arbitrary order 2D virtual elements for polygonal meshes: Part I, elastic problem, Computational Mechanics 60 (2017) 355–377.

[18] L. Beirão da Veiga, C. Lovadina, D. Mora, A virtual element method for elastic and inelastic problems on polytope meshes, Computer Methods in Applied Mechanics and Engineering 295 (2015) 327–346.

[19] E. Artioli, R. Taylor, VEM for inelastic solids, Computational Methods in Applied Sciences 46 (2018) 381–394.

[20] P. Wriggers, B. Hudobivnik, A low order virtual element formulation for finite elasto-plastic deformations, Computer Methods in Applied Mechanics and Engineering 327 (2017) 459 – 477.

[21] M. L. D. Bellis, P. Wriggers, B. Hudobivnik, G. Zavarise, Virtual element formulation for isotropic damage, Finite Elements in Analysis and Design 144 (2018) 38 – 48.

[22] E. Artioli, L. Beirão da Veiga, C. Lovadina, E. Sacco, Arbitrary order 2D virtual elements for polygonal meshes: Part II, inelastic problem, Computational Mechanics 60 (2017) 643–657.

[23] A. L. Gain, G. H. Paulino, S. D. Leonardo, I. F. M. Menezes, Topology optimization using polytopes, Comput. Methods Appl. Mech. Engrg. 293 (2015) 411 – 430.

[24] P. F. Antonietti, M. Bruggi, S. Scacchi, M. Verani, On the virtual element method for topology optimization on polygonal meshes: a numerical study, Comput. Math. Appl. 74 (5) (2017) 1091–1109.

[25] E. Artioli, Asymptotic homogenization of fibre-reinforced composites: a virtual element method approach, Meccanica 53 (2018) 1187–1201.

[26] M. Pingaro, P. Trovalusci, E. Reccia, Integrated procedure for homogenization of particle random composites using virtual element method, in:

Proceeding of XXIII Congr. Naz. AIMETA, Salerno (Italy), 4-7 September, 2017.

[27] M. Pingaro, E. Reccia, P. Trovalusci, R. Masiani, Fast statistical homogenization procedure (FSHP) for particle random composites using virtual element method, Submitted for publication – (2018) 1–10.

[28] E. Artioli, S. Marfia, E. Sacco, Virtual element technique for computational homogenization problems, in: Proceeding of XXIII Congr. Naz. AIMETA, Salerno (Italy), 4-7 September, 2017.

[29] L. Beirão da Veiga, A. Russo, G. Vacca, The virtual element method with curved edges, ESAIM: Math. Mod. Numer. Anal. 53 (2) (2019) 375–404.

[30] E. Artioli, L. Beirão da Veiga, F. Dassi, Curvilinear virtual elements for 2D solid mechanics applications, in press on Comp. Meth. Apple. Mech. Engrg.

[31] Z. Hashin, The spherical inclusion with imperfect interface, J. Appl. Mech. 58 (1991) 444–449.

[32] D. Bigoni, S. K. Serkov, M. Valentini, A. B. Movchan, Asymptotic models of dilute composites with imperfectly bonded inclusions, Int. J. Solids Struct. 35 (24) (1998) 3239–3258.

[33] A. Sommariva, M. Vianello, Gauss-green cubature and moment computation over arbitrary geometries, J. Comput. App. Math. 231 (2009) 886–896.

[34] E. Artioli, A. Sommariva, M. Vianello, Algebraic cubature on polygonal elements with a circular edge, In press on Comp. and Math. with Appl.

[35] A. Cangiani, E. H. Georgoulis, T. Pryer, O. J. Sutton, A posteriori error estimates for the virtual element method, Numer. Math. 137 (4) (2017) 857–893.

[36] S. Berrone, A. Borio, A residual *a posteriori* error estimate for the Virtual Element Method, Math. Models Methods Appl. Sci. 27 (8) (2017) 1423–1458.

[37] D. Mora, G. Rivera, R. Rodríguez, A virtual element method for the steklov eigenvalue problem, Math. Models Methods Appl. Sci. 25 (08) (2015) 1421–1445.

[38] R. Verfürth, A posteriori error estimation techniques for finite element methods, Numerical Mathematics and Scientific Computation, Oxford University Press, Oxford, 2013.

[39] Beirão da Veiga, L., Manzini, G., Residual a posteriori error estimation for the virtual element method for elliptic problems, ESAIM: Math. Mod. Numer. Anal. 49 (2) (2015) 577–599.

[40] P. F. Antonietti, L. Beirão da Veiga, C. Lovadina, M. Verani, Hierarchical a posteriori error estimators for the mimetic discretization of elliptic problems, SIAM J. Numer. Anal. 51 (1) (2013) 654–675.

[41] R. H. Nochetto, A. Veeser, Primer of adaptive finite element methods, in: Multiscale and adaptivity: modeling, numerics and applications, Vol. 2040 of Lecture Notes in Math., Springer, Heidelberg, 2012, pp. 125–225.

[42] E. Artioli, P. Bisegna, F. Maceri, Effective longitudinal shear moduli of periodic fibre-reinforced composites with radially-graded fibres, Int. J. Solids Struct. 47 (2010) 383–397.

[43] P.-A. Raviart, J.-M. Thomas, Introduction à l'analyse numérique des équations aux dérivées partielles, Collection Mathématiques Appliquées pour la Maîtrise. [Collection of Applied Mathematics for the Master's Degree], Masson, Paris, 1983.

[44] T. Kanit, S. Forest, I. Galliet, V. Mounoury, D. Jeulin, Determination of the size of the representative volume element for random composites: statistical and numerical approach, Int. J. Solids Struct. 40 (2003) 3647–3679.

MOX Technical Reports, last issues

Dipartimento di Matematica
Politecnico di Milano, Via Bonardi 9 - 20133 Milano (Italy)

04/2020 Didkovskyi, O.; Azzone, G.; Menafoglio A.; Secchi P.
Social and material vulnerability in the face of seismic hazard: an analysis of the Italian case

02/2020 Fresca, S.; Dede', L.; Manzoni, A.
A comprehensive deep learning-based approach to reduced order modeling of nonlinear time-dependent parametrized PDEs

03/2020 Ferro, N.; Micheletti, S.; Perotto, S.
Compliance-stress constrained mass minimization for topology optimization on anisotropic meshes

01/2020 Pozzi, S.; Vergara, C.
Mathematical and numerical models of atherosclerotic plaque progression in carotid arteries

56/2019 Antonietti, P.F.; Berrone, S.; Borio A.; D'Auria A.; Verani, M.; Weisser, S.
Anisotropic a posteriori error estimate for the Virtual Element Method

57/2019 Antonietti, P.F.; Bertoluzza, S.; Prada, D.; Verani M.
The Virtual Element Method for a Minimal Surface Problem

58/2019 Antonietti, P.F; Manzini, G.; Mourad, H.M.; Verani, M.
The virtual element method for linear elastodynamics models. Design, analysis, and implementation

60/2019 Ieva, F; Paganoni, A.M.; Romo, J.; Tarabelloni, N.
roahd Package: Robust Analysis of High Dimensional Data

54/2019 Simona, A.; Bonaventura, L; de Falco, C.; Schoeps, S.
IsoGeometric Approximations for Electromagnetic Problems in Axisymmetric Domains

55/2019 Agosti, A.; Ciarletta, P.; Garcke, H.; Hinze, M.
Learning patient-specific parameters for a diffuse interface glioblastoma model from neuroimaging data